NJC

Accepted Manuscript

This article can be cited before page numbers have been issued, to do this please use: B. L. Ruiz-Herrera, M. Flores-Alamo, R. A. Toscano, R. ESCUDERO and M. E. Sosa-Torres, *New J. Chem.*, 2016, DOI: 10.1039/C6NJ01621A.

View Article Online
DOI: 10.1039/C6NJ01621A

New Journal of Chemistry

ARTICLE

Adsorption of water induces a reversible structural phase transition and colour change in new nickel (II) macrocyclic complexes forming flexible supramolecular networks

Received 00th January 20xx,
Accepted 00th January 20xx

DOI: 10.1039/x0xx00000x

www.rsc.org/

Brenda Lizette Ruiz-Herrera[a], Marcos Flores-Álamo[b], Rubén Alfredo Toscano[c], Roberto Escudero[a], Martha Elena Sosa-Torres[b]*

Two novel 3D flexible supramolecular networks $[Ni_2(tpmc)(\mu\text{-}NO_3)](NO_3)_3(H_2O)_2[LiNO_3{\cdot}3H_2O]$ (**1**) and $Ni_2(tpmc)(\mu\text{-}NO_3)]_2[Ni_2(tpmc)(\mu\text{-}NO_3)Li(NO_3)_2OH]_2(LiOH(H_2O)_3)_2(NO_3)_8(H_2O)_{13}{\bullet}nH_2O$ (**2**) (*tpmc*, 1,4,8,11-tetrakis-(2-pyridylmethylene)-1,4,8,11-tetraaza cyclotetradecane) were synthetised and characterized by spectroscopic and X-ray techniques. Their single crystal X-ray diffraction analysis showed that, in both compounds, nickel (II) ions are in an octahedral environment, due to an unusual binding mode of nitrate, acting as either tetradentaded ligand in **1**, or as a pentadentated ligand in **2**. The blue compound **1** adsorbs water leading to the violet compound **2**. The adsorption of water leads to a reversible crystal-to-crystal structural phase transition, from the monoclinic structure of **1**, to the triclinic structure of **2**. Phenomenon that was corroborated by XRPD. This phase transition is accompanied by a reversible reaction of ligand exchange responsable for the color-change observed in the compounds, property which might be useful for the development of molecular sensors. Adsorption-desorption isotherms at low and high pressure indicated **1** has capacity of gas adsorption, such as dinitrogen, dioxygen, or carbon dioxide. Besides, dynamic water vapour isotherms confirm a chemisorption highly selective for water vapor. This is the first time Ni (II) – *tpmc* complex has been observed to be involved in a reversible gas adsorption process, furthermore, herein we report the first crystal structures of six-coordinated nickel (II) complexes with *tpmc*.

Introduction

Numerous heterocyclic multidendate ligands and their transition metal complexes have been used as building blocks and templates for the design of functional materials. [1, 2] Such supramolecular compounds include host-guest systems, molecular devices, self-assemblies, stimuli-sensitive materials, and nanoscale structures. [3] Within this, flexible solids are functional materials that can be either coordination or supramolecular networks. They possess flexible cavities able to adsorb a wide variety of molecules, performing reversible structural transformations, induced by the adsorption and removal of guest molecules. [4] In particular, flexible solids are involved in gas storage and sensing, in which water adsorption is especially important for technological applications, such as the design of water-delivering devices and adsorption-driven heat exchangers also known as thermal batteries, as well as their application as air-conditioning units in vehicles, or as dehumidifiers.[4, 5]

We chose 1,4,8,11-tetrakis-(2-pyridylmethylene)-1,4,8,11-tetraazacyclotetradecane (*tpmc*), as base for our compounds. *Tpmc* is a macrocyclic ligand well known for its ability to form stable complexes with transition metals in lower oxidation states, *e.g.*, copper (II), cobalt (II) and nickel (II), among others. [6-10] In these binuclear complexes, the metal ion remained exo-coordinated from the macrocycle, where *tpmc* can adopt either a chair or a boat conformation depending on the metal ion and the nature (mono or polydentate) of a secondary ligand bound to the metal centers.[6, 7] Figure 1 shows the tetraazamacrocycle *tpmc* and its conformational structures adopted in binuclear compounds.

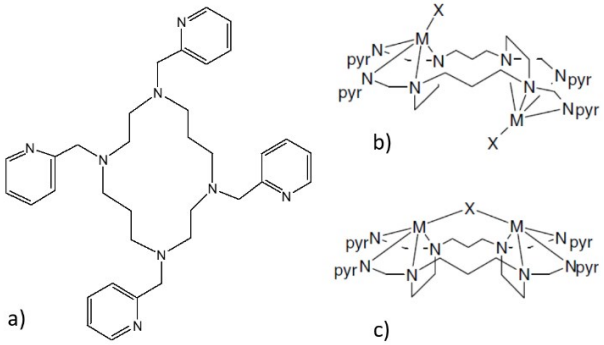

Fig. 1: a) Representation of the 1,4,8,11-tetrakis-(2-pyridyl methylene)-1,4,8,11-tetraazacyclotetradecane (*tpmc*), b) chair structure and c) boat structure.

[a] Instituto de Investigaciones en Materiales,
[b] Departamento de Química Inorgánica y Nuclear, Facultad de Química,
[c] Instituto de Química. Universidad Nacional Autónoma de México, Ciudad Universitaria, México, D.F. 04510, México. * E- mail: mest@unam.mx

†Electronic Supplementary Information (ESI) available contains additional infrared spectra, further representation of crystal structures, and additional measurements related to water adsorption. The crystallographic data for the structures reported in this paper have been deposited with the Cambridge Crystallographic Data Centre, CCDC numbers: 1406400 and 1406401. See DOI: 10.1039/x0xx00000x.

Like other tetraazamacrocyclic ligands, *tpmc* coordinates each metal ion by the two cyclam ring nitrogens and by two donor atoms of the pendant groups, leaving one of the axial positions open for a secondary ligand, while the other position is sterically blocked by the pendant groups. This arrangement explains the preference for five-coordinated structures.[7, 11-12] Nevertheless, six-coordinated structures of metal complexes with tetraazamacrocycles become feasible when using an appropriate secondary ligand. For example, Co(II) and Ni(II) complexes with 1,4,8,11-tetrakis-(2-aminoethyl)-1,4,8,11-tetraazacyclotetradecane (*taec*) show octahedrally distorted metal sites, with carbonate as secondary ligand. Hereby, the carbonate anion acts as a bridging ligand in a symmetrical bidentate way.[11, 12] So far, crystal structures of analogous *tpmc* complexes have not been reported, however, infrared and electronic spectra of $[Co_2CO_3(tpmc)](ClO_4)_2{\cdot}2H_2O$ and $[Co_2CO_3(tpmc)](BF_4)_2{\cdot}2H_2O$ suggest the presence of six-coordinated Co(II) sites. Surprisingly, in view of the numerous crystal structures of $[M_2(tpmc)L]$ complexes, structures of corresponding Ni(II) complexes have not been reported to date,[13] even though Ni(II)-*tpmc* complexes are known since many years.[9]

Here we describe the functional and structural characterization of two new $Ni_2(tpmc)$ complexes **1** and **2**, with nitrate as secondary ligand, stabilizing hexa-coordinated Ni(II) centers. The compounds form flexible supramolecular solids involved in a reversibly adsorption-desorption water process. The change in the hydrogen bonding network caused by the inclusion of water, induced a structural phase transition, from monoclinic to triclinic, accompanied by a reversible ligand exchange. This results in a remarkable color change, from blue (complex **1**) to violet (complex **2**), property which might be useful for the development of molecular sensors.

Experimental

Materials and methods

Commercially available reagents were used without further purification, gases were from Praxair. Fourier Transformed Infrared spectra were recorded on a Perkin-Elmer 400 FT-IR/FT-FIR spectrophotometer, over the range 4,000 to 400 cm^{-1} (attenuated total reflectance mode), and for the range of 600 to 50 cm^{-1} (polyethylene pellets windows). Electronic absorption spectra were measured on a Carry - 5E Varian spectrometer over the range 40,000 - 4,000 cm^{-1} on the diffuse reflectance mode. Elemental analyses were carried out on a Perkin-Elmer 2400 microanalyser, using L-cystine as standard.

Synthesis of *tpmc*

The ligand 1,4,8,11-tetrakis-(2-pyridylmethylene)-1,4,8,11-tetraazacyclotetradecane (*tpmc*) was prepared following the reported procedure; its characterization by ^{1}H-NMR and elemental analysis agree with reported values. [10]

Synthesis of $[Ni_2(tpmc)(\mu\text{-}NO_3)](NO_3)_3(H_2O)_2[LiNO_3{\cdot}3H_2O]$: 1

A solution of *tpmc* (0.5 g, 0.88 mmol) and LiOH (0.048g, 2.0 mmol) in anhydrous ethanol was stirred under nitrogen gas flux during 10 minutes. Hereafter, a solution of $Ni(NO_3)_2{\cdot}6H_2O$ (0.52 g, 1.77 mmol) in anhydrous ethanol, was added dropwise to the ligand solution over a period of 1 h. The mixture was refluxed under nitrogen for 20 h. The blue precipitate was collected by filtration, washed with a minimum amount of dry dichloromethane, and finally dried under dinitrogen atmosphere, giving the blue complex **1**, $[Ni_2(tpmc)(\mu\text{-}NO_3)](NO_3)_3{\cdot}(H_2O)_2[LiNO_3{\cdot}3H_2O]$; Anal. Calc. for $Ni_2C_{34}N_{13}H_{54}O_{20}Li$ (%): C, 37.49; H, 4.99; N, 16.72; Found: C, 37.76 ± 1.79; H, 3.63 ± 1.37; N, 15.59 ± 0.56. The presence of lithium, which comes from the reactants, was confirmed by the lithium flame test.[14]

Synthesis of $[Ni_2(tpmc)(\mu\text{-}NO_3)]_2[Ni_2(tpmc)(\mu\text{-}NO_3)Li(NO_3)_2OH]_2(LiOH(H_2O)_3)_2(NO_3)_8(H_2O)_{13}{\bullet}nH_2O$: 2

Exposure of complex **1** to ambient laboratory conditions leads to the violet complex **2**: $[Ni_2(tpmc)(\mu\text{-}NO_3)]_2[Ni_2(tpmc)(\mu\text{-}NO_3)Li(NO_3)_2OH]_2(LiOH(H_2O)_3)_2(NO_3)_8(H_2O)_{13}{\bullet}nH_2O$; where n = 32. Anal. Calc. for $Ni_8C_{136}N_{48}H_{282}O_{103}Li_4$ (%): C, 34.49; H, 6.00; N, 14.19; Found: C, 34.63 ± 0.65; H, 4.80 ± 0.41; N, 14.14 ± 0.26.

Additionally, **2** was obtained, exposing **1** to deuterated water vapour, using deuterium oxide (99.9 atom %D) from Aldrich.

X-ray diffraction (XRD) crystal analysis

Suitable crystals of complex **1** were obtained from the original reaction mixture prior to the filtration step. A small amount of the solution was kept at room temperature to allow slow evaporation, giving blue crystals of complex **1**. After an aging period, the blue crystals turned into the violet crystals of complex **2**.

The structure of complex **1** was determined at 120 K on the Oxford Diffraction Gemini "A" diffractometer, equipped with a CCD area detector, a sealed tube X-ray radiation source ($\lambda_{MoK\alpha}$ = 0.71073 Å), and a graphite monochromator. The CrysAlisPro and CrysAlis RED software packages were used for data collection and data integration.[15] Analysis of the integrated data did not reveal any crystal decay. Final cell constants were determined by a global refinement of 5583 ($3.462 < \theta < 29.565$ °) and collected data were corrected for absorption effects.

The structure of complex **2** was determined on the Bruker Smart Apex diffractometer, using Mo-Kα radiation, a graphite-monochromator, and ω scans at 150 K. The intensities were integrated using SAINT, absorption correction and scaling was performed with SADABS.[16]

Both structures were solved with the program SHELXS97; the full-matrix least-squares refinement was achieved with SHELXL97 for complex **1** and SHELXL-2014 for complex **2**. [17] All atoms except hydrogen were refined anisotropically. The hydrogen atoms of water were located in a difference Fourier map and refined isotropically with Uiso(H) = 1.5 Ueq for (O). H atoms attached to C atoms were placed in geometrically

View Article Online
DOI: 10.1039/C6NJ01631A

idealized positions and refined by a riding model with isotropic displacement parameters tied to the parent carbon atoms. ORTEP-3 for Windows was employed for molecular graphics.[18] Finally, the programs CCDC MERCURY and Diamond 4.0 were used to prepare material for publication.[19]

Many efforts to refine the structure of compound **2** in the triclinic space group P-1 were unsuccessful, that is why, the structure was refined in the triclinic space group P1, which reveals a clearly overall centrosymmetric arrangement, quantified by the PLATON-ADDSYM routine in 92%. The presence of additional (Non) Crystallographic glide plane between Ni cations was also detected by the PLATON-NONSYM routine.

X-Ray powder diffraction (XRPD) analysis

Data were obtained on a Bruker D-8 Discover diffractometer with the Bragg-Brentano θ-θ configuration, equipped with a Cu-Kα radiation source, a Ni (0.5%) Cu-Kβ filter in the secondary beam, and a one-dimensional position-sensitive silicon strip detector (Bruker, Lynxeye). XRPD patterns were obtained under vacuum in a sealed sample holder at 298 K; this temperature was gradually increased to 353 K with the Anton-Paar HTK 1200N high-temperature oven chamber. In all cases, the diffraction intensity as a function of 2θ angles was measured between 4.001 and 109.98°, with a 2θ step of 0.019447°, for 264 s per point. Diffraction patterns were indexed with the software EXPO2014. [20]

Analysis of functional properties

The complexes were investigated by thermogravimetric analysis, BET adsorption-desorption and water-vapour isotherms and scanning electron microscopy coupled to Energy-dispersive X-ray spectroscopy (SEM-EDS).

Thermogravimetric analyses were performed under dinitrogen (grade 5.0), with a heating rate of 5 °C/min (278 $Kmin^{-1}$) in a thermobalance Mettler-Toledo model TGA/SDTA851^e.

Isotherms at low relative-pressure, under nitrogen, were acquired on a Bel-Japan Minisorp II at 77 K, by using a multipoint technique. Samples were degassed at 353 K for 20 h under vacuum prior to the analysis. Data were analysed applying the Brunauer-Emmett-Teller (BET) and the Barrett-Joyner-Halenda (BJH) models. [21] Isotherms at high pressure, under CO_2, were obtained on a volumetric Belsorp-HP instrument from Bel-Japan. The equipment performs additional degassing of the sample by applying vacuum. Experiments were performed between atmospheric and 4.5 MPa of pressure, at 303.5 K.

Dynamic water adsorption/desorption studies were carried out on a Q5000SA thermobalance from TA Instruments (associated error of 0.1 wt %), equipped with a humidity and temperature controlled chamber (associated error of 0.1 % of relative humidity). Prior to the measurements the samples were degassed (vacuum, 353 K, 20 h). Measurements were performed using distilled water and carrier gases dinitrogen (grade 4.8), carbon dioxide (3.0) and dioxygen (2.6). The total gas flow rate was 100 mL/min, and the relative humidity (RH) percentages were automatically controlled by the instrument.

The morphology and element composition of complexes were determined on a JEOL JMS-7600F SEM-EDS instrument.

Results and discussion

Reversible switching between compounds 1 and 2

The reaction between $Ni(NO_3)_2{\cdot}6H_2O$ and *tpmc* in anhydrous ethanol produced the blue Ni(II) complex **1** when performed under dinitrogen. Upon exposure to air (ambient laboratory environment) complex **1** was transformed to the violet complex **2**. To get further insight into these findings, the reaction was repeated several times recovering the product under different atmospheres: carbon dioxide, dioxygen or water vapor. It was found that the observed colour-change is the result of an adsorption phenomenon of water vapour. Phenomenon that is reversible even after several cycles. Moreover, it is easy to interchange between the two complexes; *i.e.* **1** can be obtained by warming **2** at 353 K for 2 h in a vacuum furnace, and **2** can be obtained exposing **1** to the environment. Figure S1 show a schematic representation of the described process.

Hexa-coordinated nickel (II) complexes with *tpmc*

The electronic solid state reflectance spectra of both complexes **1** and **2** (figure 2) revealed features consistent with an octahedral environment of Ni(II) (d^8).[22] For complex **1**, the first maximum at 968 nm (10,330 cm^{-1}) corresponds to the transition $^3A_{2g} \rightarrow {}^3T_{2g}$ (F) (ν^1); the second, at 575 nm (17,402 cm^{-1}), to $^3A_{2g} \rightarrow {}^3T_{1g}$ (F) (ν^2); and the third, at 375 nm (26,667 cm^{-1}), to $^3A_{2g} \rightarrow {}^3T_{1g}$ (P) (ν^3). In the case of compound **2**, the corresponding transitions are at 952 nm (10,507 cm^{-1}) with a shoulder at 890 nm (11231 cm^{-1}), 569 nm (17,575 cm^{-1}) and 368 nm (27,152 cm^{-1}). The maxima of complex **2** are slightly shifted to higher energies consistent with the observed colour change from blue to violet.

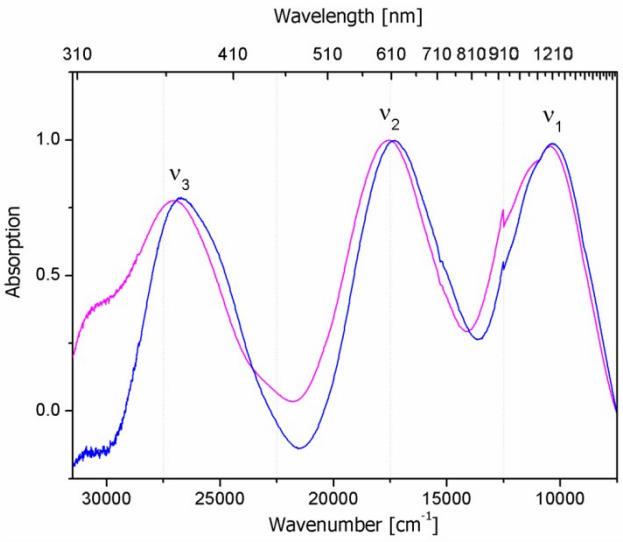

Fig. 2: Electronic spectra of Ni(II) complexes: **1** (blue line) and **2** (violet line).

View Article Online
DOI: 10.1039/C6NJ01624A

Ni (II) - *tpmc* complexes differentiated by infrared spectroscopy

Mid-infrared spectra (vs, very strong; s: strong; m: medium; w: weak intensity) of complexes **1** and **2** (figure S2, ESI†) revealed maxima at 2924 cm^{-1} (m) and 2891 cm^{-1} (m) for $\nu(CH_2)$, 1610 cm^{-1} (s) and 1574 cm^{-1} (m) for ν(C=N), as well as a maximum characteristic of mono-substituted pyridines at 760 cm^{-1} (s). [23] These maxima are shifted relative to those of the free ligand, in agreement with previously reported data of *tpmc* comlexes.[7, 9]

Besides, there are a maxima which can be assigned to a coordinated nitrate anion,[24] at 1483 cm^{-1} (vs) [$\nu_s(NO_3)$], 1277 cm^{-1} (vs) [$\nu_1(NO_3)$] and 1027 cm^{-1} (s) [$\nu_2(NO_3)$] for complex **1**, compared to 1511 cm^{-1} (vs) [$\nu_s(NO_3)$], 1272 cm^{-1} (vs) [$\nu_1(NO_3)$] and 1025 cm^{-1} (s) [$\nu_2(NO_3)$] for **2**. The difference $\Delta(\nu_s\text{-}\nu_1)(NO_3)$ of 206 cm^{-1} (complex **1**) and 239 cm^{-1} (complex **2**) originates from a chelating nitrate ligand, whereas the maximum at 1335 cm^{-1} (vs) is assigned to nitrate anions not involved in metal binding. [23, 24]

Finally, the mid IR spectra of complexes **1** and **2** differ with regard to characteristic bands resulting from lattice water.[23] Compound **2** shows a maximum at 3400 cm^{-1} which is assigned to the stretching H-O-H vibration mode, with the corresponding bending vibration maximum at 1640 cm^{-1}. These features are absent in the spectrum of compound **1**.

Far infrared spectra of complexes **1** and **2** (figure 3) show a band centered at 270 cm^{-1} [ν_s(M-O, NO_3)] consistent with a coordinated nitrate,[23, 24] the second maximum at 420 cm^{-1} has been assigned to [ν_s(M-N, NO_3)].[13] In the spectrum of complex **2** there are two additional maxima at 537 and 574 cm^{-1}, which are absent in the spectrum of complex **1**.

The origin of these bands has been discussed controversially in the literature, they were either assigned to the M-O bond of a coordinated water molecule (ν(M-O,H_2O)), or to the M-O bond of a coordinated nitrate anion (ν(M-O, NO_3^-)). [24] In order to assign these bands, complex **2** was produced by exposure of complex **1** to D_2O vapour.

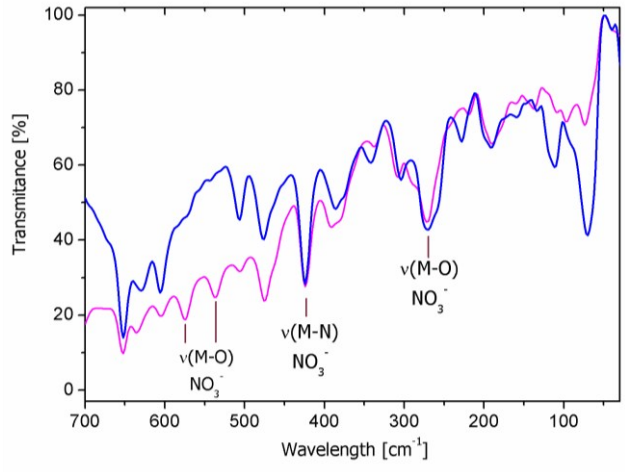

Fig. 3: Far-infrared spectra of Ni(II) complexes: **1** (blue line) and **2** (violet line), showing the position and assignment of the individual bands.

The resulting mid infrared spectrum of deuterated complex **2** (figure S3a, ESI†)) revealed the expected shift from 3,400 to 2,523 cm^{-1} for the D-O-D stretching vibration[23]. While in the far infrared spectrum (figure S3b, ESI†) none of the bands were shifted. Thus, the bands, at 537 and at 574 cm^{-1}, were assigned to coordinated nitrates.

Crystal structures of complexes 1 and 2

Blue crystals of **1**, suitable for single-crystal X-ray diffraction, were obtained directly from the reaction mixture. When these crystals were exposed to ambient laboratory conditions for several days, the violet crystals of **2** were obtained. Crystallographic parameters are compiled in Table 1.

Table 1. Crystal data and structure refinement for complexes **1** and **2**.

Compound	**1**	**2**
Empirical formula	C34 H54 Li N13 Ni2 O20	C136 H218 Li4 N48 Ni8 O71
Formula weight	1089.26	4159.01
Temperature	120(2) K	150(2) K
Crystal system	Monoclinic	Triclinic
Space group	$P\,2_1/n$	$P\,1$
Unit cell dimensions	a = 11.2417(7) Å b = 18.3142(11) Å c = 22.6389(13) Å α = 90 ° β = 101.822(6) ° γ = 90 °	a = 11.2964(8) Å b = 18.8819(14) Å c = 20.7624(13) Å α = 87.453(5)° β = 89.238(4)° γ = 83.960(5)°
Volume	4562.1(5) $Å^3$	4399.5(5) $Å^3$
Z	4	1
Density (calculated)	1.586 Mg/m^3	1.570 Mg/m^3
Absorption coefficient	0.918 mm^{-1}	0.944 mm^{-1}
F(000)	2272	2174
Crystal size / colour / shape	0.58 x 0.20 x 0.19 mm / blue / prism	0.383 x 0.229 x 0.196 mm / violet / prism
Theta range for data collection	3.462 to 29.565°	1.432 to 27.641°
Index ranges	-11<=h<=14, -12<=k<=23, -29<=l<=31	$-14 \le h \le 11$, $-24 \le k \le 24$, $-26 \le l \le 26$
Reflections collected	23469	43154
Independent reflections	10724 [R(int) = 0.0323]	28357 [*R*(int) = 0.0498]
Completeness to theta	99.8 % (θ= 25.242°)	99.3 % (θ= 25.242°)
Refinement method	Full-matrix least-squares on F^2	Full-matrix least-squares on F^2
Data / restraints / parameters	10724 / 0 / 655	28357 / 83 / 2524
Goodness-of-fit on F^2	1.040	1.015
Final R indices [I>2sigma(I)]	R1 = 0.0586, wR2 = 0.1470	*R*1 = 0.0624, *wR*2 = 0.1551
R indices (all data)	R1 = 0.0825, wR2 = 0.1661	*R*1 = 0.0844, *wR*2 = 0.1699
Extinction coefficient	n/a	----
Absolute structure parameter	-----	0.423(12)
Largest diff. Peak and hole	1.979 and -0.912 e.$Å^{-3}$	0.699 and -1.998 e.$Å^{-3}$

View Article Online
DOI: 10.1039/C6NJ01621A

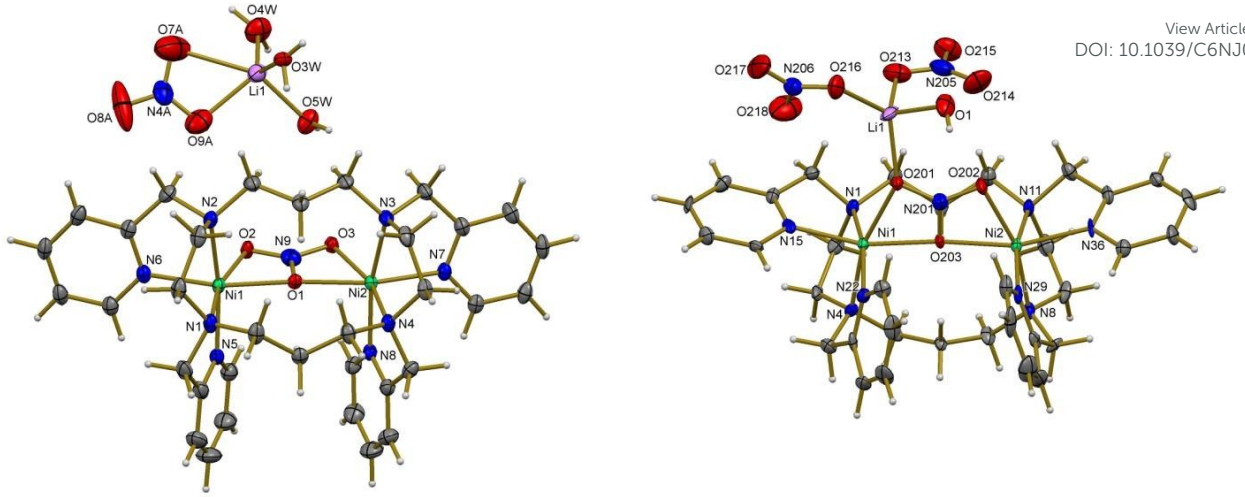

Fig. 4: Structural comparison between cations present in compounds **1** (left) and **2** (right). Perspective view of the molecular structures, C (black); H (white); O (red); N (blue); Ni (green) and Li (pink). Thermal ellipsoids are shown at the 50% probability level

Ni(II) complex **1** crystallized in a monoclinic structure with a space group $P2_1/n$. The asymmetric unit was formed by one $[Ni_2(tpmc)(\mu\text{-}NO_3)]^{3+}$ cation, three nitrate anions, two water molecules and one $Li(NO_3)(H_2O)_3$ unit (figure S4).

A perspective view of the molecular structure of the $[Ni_2(tpmc)(\mu\text{-}NO_3)]^{3+}$ cation in compound **1** is shown in figure 4 (left). Nickel ions are bridged by a *tpmc* ligand and by a nitrate. As in previous *tpmc* complexes, [7-10] the octadentate ligand is coordinated to the two nickel (II) ions through the nitrogen atoms of the four pendant pyridine rings and through the four nitrogen atoms of the macrocycle. Metal centres are exo-coordinated, out of the *cyclam* ring which adopts a *SRSR*(*RSRS*) configuration. Added to this, the coordination mode of the nitrate anion gives an octahedral geometry for the nickel atoms, consistent with the electronic spectrum of the compound. In this environment one macrocyclic amine, one methylpyridine and two of the oxygen atoms of the nitrate group occupy an equatorial plane, while the remaining macrocyclic amine and methylpyridine pendant occupy the apical positions for each nickel (II) ion. The found Ni – N bond lengths in complex **1**, 2.049(3) to 2.147(3) Å, are within the expected range, according to the bond lengths of analogous cobalt and copper complexes. [7-10, 25] Table S1 lists the selected bond distances and angles for complex **1**.

A further description of the nitrate ligand, indicates, it behaves as a tetradentate bridging ligand, connecting the two nickel (II) centres in a bis-bidentate way.[26] This can be described as μ^2-nitrate-1κ^1O,2κ^1O,3κ^2O; which means two oxygen atoms from the nitrate ligand are coordinated each to one of the two nickel (II) ions, while the third oxygen is bonded to both metal centres. [27]

There are few examples of this coordination by a nitrate anion. [26, 28, 29] An equivalent coordination mode was observed for a carbonate anion in the binuclear nickel (II) complex with the ligand *taec*.[12] In which the μ-carbonate-bridge ligand is bound to the metals centres by its oxygens, in the same way as our nitrate bridges the nickel (II) ions. The distorted octahedral geometry of the metal centres in complex **1** results from the presence of this symmetrically bidentate ligand. The O-Ni-O angles (62.15(9) and 62.69 (9)°) in complex **1**, show the deviation of the ideal octahedral geometry. Table S1 compiles the main bond lengths and angles of compound **1**.

The lithium site in $Li(NO_3)(H_2O)_3$ present in complex **1** shows a pentacoordinated Li^+ cation in a distorted trigonal bipyramidal geometry, formed by three water molecules and one chelating nitrate anion. Such coordination is rather uncommon for lithium and has mostly been observed in organometallic lithium compouds [30-32] and in LiB_6O_9F, the first reported lithium fluorooxoborate.[33] Accordingly, the mean Li-O distance (1.921(8) to 2.429(9)) in complex **1**, is in agreement with the distances observed in these previous reported compounds (see Table S2).

Figure 5 shows the crystal lattice of **1**, where the intermolecular interactions through hydrogen bonding can be observed around the binuclear nickel complexes. In general, these interactions form a $D_2^2(5)$, $D_2^2(7)$ and $R_2^2(8)$ graphical set, [34] corresponding to chains and rings where two donor atoms and two acceptors form the hydrogen bonding, leading to a three-dimensional supramolecular architecture, that gives structural stability to the network of complex **1**. Table 2 summarizes the main hydrogen bonding interactions present in the compound **1**.

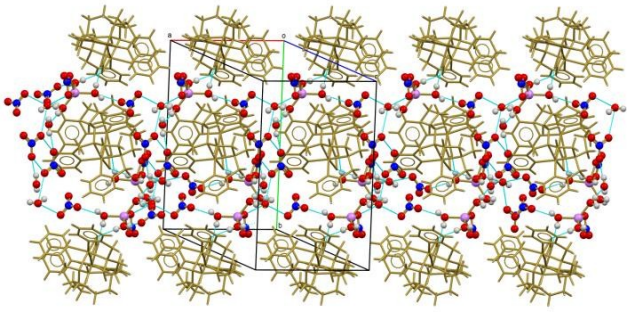

Fig. 5: Crystal lattice of complex **1** along plane *a*-*b*. Intermolecular hydrogen bond interactions are marked in green.

Table 2. Hydrogen bonding interactions in complexes **1** and **2**

Complex **1**

Donor-H···Acceptor	D - H [Å]	H···A [Å]	D···A [Å]	D - H···A [°]
O(3W)-H(3WA)...O(2)[a]	0.80(10)	1.92(10)	2.721(4)	172(9)
O(3W)-H(3WB)...O(1A)[b]	0.78(10)	2.11(9)	2.842(5)	158(10)
O(4W)-H(4WA)...O(11A)[c]	0.96(9)	1.88(9)	2.825(6)	166(8)
O(5W)-H(5WB)...O(3)[a]	0.85(9)	1.98(9)	2.824(4)	173(9)

Symmetry transformations used to generate equivalent atoms:
a) -x+2,-y+1,-z+1; b) x+1/2,-y+3/2,z+1/2; c) -x+3/2,y+1/2,-z+3/2

Complex **2**

Donor-H···Acceptor	D - H [Å]	H···A [Å]	D···A [Å]	D - H···A [°]
O(1)-H(1)...O(227)	0.818(13)	2.07(5)	2.815(14)	150(9)
O(7)-H(7C)...O(215)	0.849(13)	2.27(4)	2.851(12)	125(4)
O(4)-H(4)...O(211)	0.826(13)	1.97(3)	2.751(9)	157(7)
O(10)-H(10C)...O(210)	0.852(13)	1.86(3)	2.684(10)	163(10)
O(13)-H(13D)...O(215)[d]	0.851(13)	2.26(11)	2.977(14)	141(15)
O(16)-H(16A)...O(217)[d]	0.848(13)	2.08(3)	2.910(13)	165(11)
O(1)-H(1)...O(227)	0.818(13)	2.07(5)	2.815(14)	150(9)

Symmetry transformations used to generate equivalent atoms:
d) x-1,y,z

The exposure of the blue crystals of complex **1** to ambient conditions produced the violet crystals of complex **2**, which crystallizes in a triclinic structure with space group P1. The unit cell of complex **2** (figure S5), consists of two types of binuclear Ni(II) cations, two lithium entities: $Li(OH)(H_2O)_3$, eight nitrate anions and thirteen water molecules. Table 1 summarizes crystallographic parameters.

One of the nickel cations in compound **2** is exactly as that one described in **1**, corresponding to the molecule $[Ni_2(tpmc)(\mu\text{-}NO_3)]^{3+}$. In the second cation, the mode of coordination of *tpmc* and the nitrate ligand is retained, but, it differs by the presence of a lithium coordinated to one of the oxygens (O201) of the bridging nitrate, resulting in the non equivalence of the nickel ions. The interatomic distance Li(1) – O(201) is 1.972(17) Å corresponding to a covalent bond. The tetrahedral geometry of this lithium attached to the oxygen of the nitrate-bridging ligand, is completed by one hydroxyl and two nitrate anions. The second cation in compound **2**, corresponds then, to the molecule $[Ni_2(tpmc)(\mu\text{-}NO_3)Li(NO_3)_2OH]^+$ shown in figure 4 (right).

A similar way, in the carbonato-bridged cobalt (II)-*taec* complex, a sodium ion is located at close proximity to one of the carbonate oxygens, suggesting a Na – O bond. [12]

The nitrate in the second cation acts as a pentadentate bridging ligand described as μ^3-nitrate-1κ^1O,2κ^2O,3κ^2O. [27] This is the first observation of this coordination mode for nitrate (see Table S1).

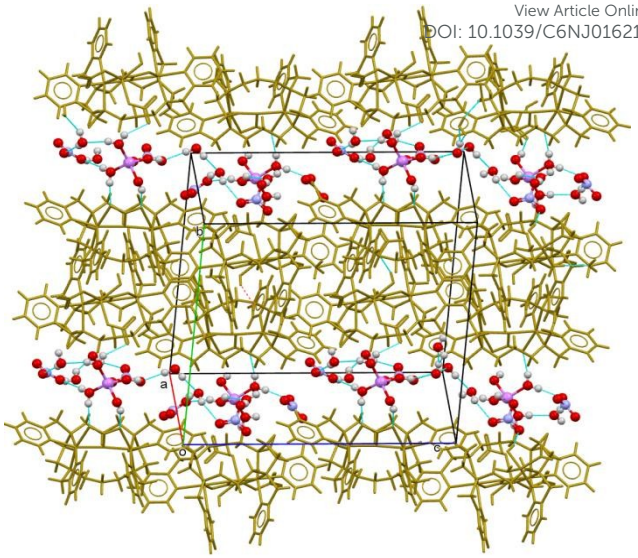

Fig. 6: Crystal lattice of complex **2**. Intermolecular hydrogen bond interactions are marked in green.

Worth is to mention that the incorporation of the lithium entity into the coordination sphere of nickel in complex **2** changes its electronic environment, resulting in the observed colour change.

The adsorption of water induces the coordination of lithium entities towards the bridging nitrate, process that is completely reversible when water is removed. This switching in the coordination sphere has been described as a reaction of ligand exchange.[35]

Crystal lattices of complexes **1** and **2** are stabilized mainly by intermolecular interactions of hydrogen bonding. The structure of **1** owns cavities and channels along the network. When the adsorption process takes place, water molecules occupy these positions, causing a distortion and expansion of the original frame, giving rise to a new lattice in complex **2**.

The crystal lattice of **2** contains water molecules distributed in open channels along the c axis (figure 6). These interactions, summarized in table 2, correspond to hydrogen bonds of the type $D_2^2(8)$, $D_2^2(9)$ and $R_2^2(8)$. [34] An additional representation of the crystal lattice of compound **2** is shown in figure S6, where the molecules involved in the hydrogen bonding are emphasised in order to get a better perspective of these supramolecular interactions.

The hydration process modifies the supramolecular networks promoting the reversible phase transition from monoclinic in **1** to triclinic structure in **2**. Figure 7 shows the reaction of reversible ligand exchange and compares different views of the supramolecular frameworks of complexes **1** and **2**, underling the importance of lithium units in the stabilization of the crystal lattices and its role in the reversible reaction of ligand exchange upon adsorption of water. Figure 8 represent a plausible motion of molecules involved in the ligand exchange reaction.

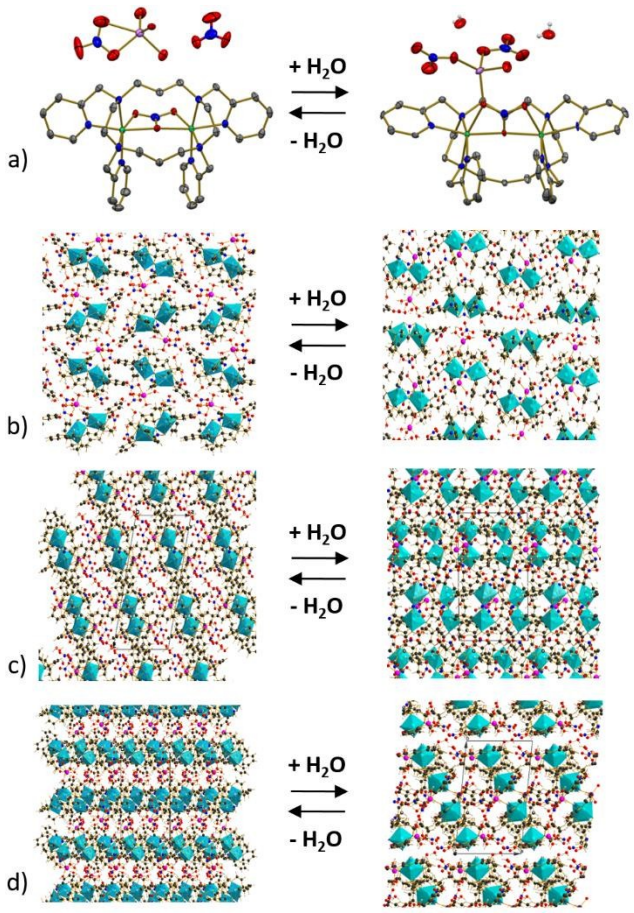

Fig. 7: Reversible ligand exchange and structural phase transition induced by water adsorption. a) Interconversion between the Ni(II)-*tpmc* cations present in compounds **1** and **2**. Perspective view of the supramolecular network of complex **1** and **2** along *a* axis (b); *b* axis (c), and *c* axis (d). Nickel polyhedrons are marked in green.

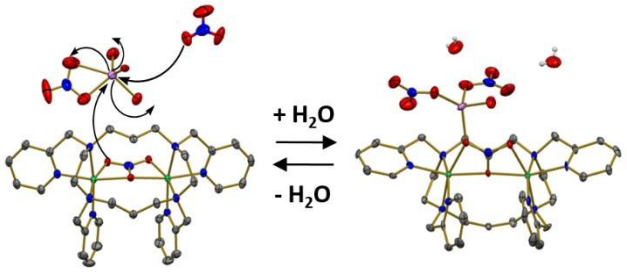

Fig. 8: Drawing of a possible motion of molecules involved in the ligand exchange reaction.

The non-equivalence of nickel atoms derived of this water-induced ligand-exchange process, explains the shift to higher energies of the bands in the electronic spectrum of compound **2** (figure 1) and the observed colour change. This also explains the differences observed in the infrared spectra of the compounds. The observed shifted to higher energies bands of complex **2**, at 1511 cm^{-1} [$\nu_s(NO_3)$], 1272 cm^{-1} (vs) [$\nu_1(NO_3)$] and 1025 cm^{-1} (s) [$\nu_2(NO_3)$] (figure S2) are in agreement with a new coordination mode of the nitrate. On other hand, in the far region (figure 3), the bands at 537 and 574 cm^{-1}, only present in spectrum of compound **2**, correspond to a second vibration mode of the oxygen-nitrate atom coordinated simultaneously to nickel and lithium atoms. These bands disappear when the sample is dehydrated, leading to compound **1**, and reappear upon adsorption of water, giving evidence of this reversible structural change.

Powder X-ray diffraction

As stated by single crystal X-ray diffraction analysis, the binuclear nickel (II) complexes here reported, undergo a crystalline-to-crystalline transformation induced by adsorption of water. This dynamic structural behaviour was verified by powder X- ray diffraction (XRPD).

When complex **2** is heated in a vacuum furnace at 353 K for two hours, complex **1** is obtained, which remains dehydrated for several days if kept under nitrogen atmosphere in a desiccator. When **1** was exposed to ambient conditions compound **2** was obtained almost immediately. Figure 9 shows the XRPD patterns of the described samples. The identity of each compound was confirmed by infrared spectroscopy and by elemental analysis. These results indicate a phase transition from a triclinic structure for compound **2** (Anal. Calc. (%): C, 34.49; H, 6.00; N, 14.19; Found: C, 34.63 ± 0.65; H, 4.80 ± 0.41; N, 14.14 ± 0.26), (fig. 9-a), to another crystalline structure, corresponding to compound **1** (Anal. Calc. (%):C, 37.49; H, 4.99; N, 16.72; Found: C, 37.76 ± 1.79; H, 3.63 ± 1.37; N, 15.59 ± 0.56), (fig. 9-b). The original crystalline phase was restored after rehydration process (fig. 9-c) producing the complex **2** $[Ni_2(tpmc)(\mu\text{-}NO_3)]_2[Ni_2(tpmc)(\mu\text{-}NO_3)Li(NO_3)_2OH]_2(LiOH(H_2O)_3)_2(NO_3)_8(H_2O)_{13}{\bullet}nH_2O$; where n = 20. (Anal. Calc. C, 36.15; H, 5.75; N, 14.87; Found: C, 36.23± 0.02; H, 5.10 ± 0.02; N, 14.96 ± 0.025)

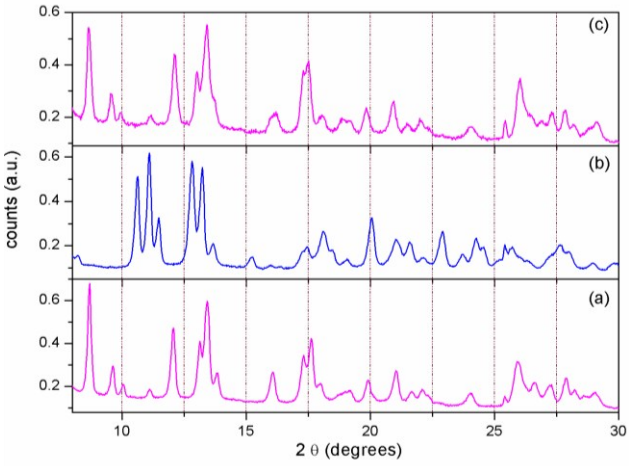

Fig. 9: XRPD patterns for complex **2** (a), complex **1** (b) and the recovered complex **2** (c).

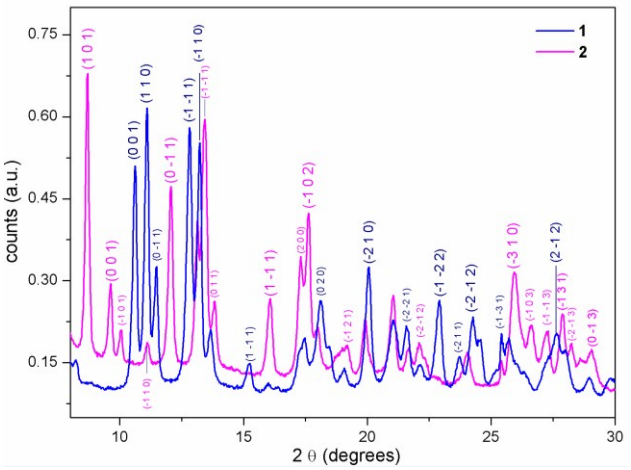

Fig. 10: Assignment of the reflexions in the XRPD patterns for complex **2** and complex **1**, and comparison between them.

Figure 10 evidences the structural phase transition by comparison between indexed reflexions of the diffraction patterns of complexes **1** and **2**. All the reflexions were assigned. [20]

Microstructural characterization and description of sorption phenomenon

Thermogravimetric (TG) and differential thermogravimetric analysis (DTG and DTA) were performed for **1** and **2**. Figure 11 shows the decomposition pattern of compound **2**. The first transition corresponds to the loss of 12.51 %w (30-180 °C) assigned to 32 molecules of water (calc. 12.20 %), confirming the formula: $[Ni_2(tpmc)(\mu\text{-}NO_3)]_2[Ni_2(tpmc)(\mu\text{-}NO_3)Li(NO_3)_2OH]_2(LiOH(H_2O)_3)_2(NO_3)_8(H_2O)_{13}\bullet 32H_2O$, found by elemental analysis. This transition corresponds to the loss of adsorbed water. At the beginning (≈ 50 °C) an abrupt change is observed, corresponding to the loss of the most superficial water. As temperature rises, the chemisorbed water is lost gradually until all water is desorbed at 180 °C.

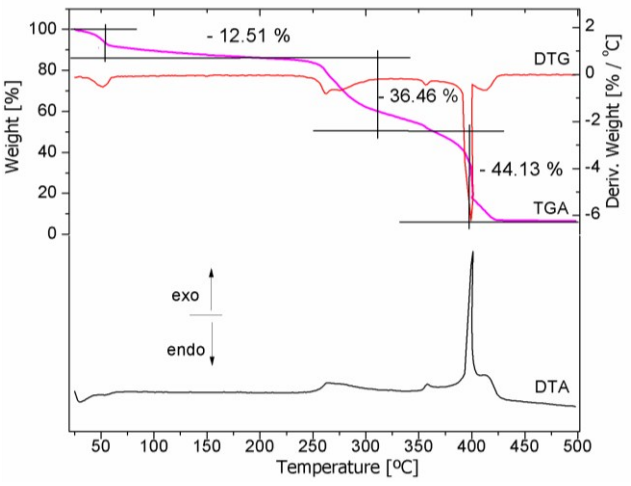

Fig. 11: Thermal analyses of **2** run under N_2 at 5 °C/min.

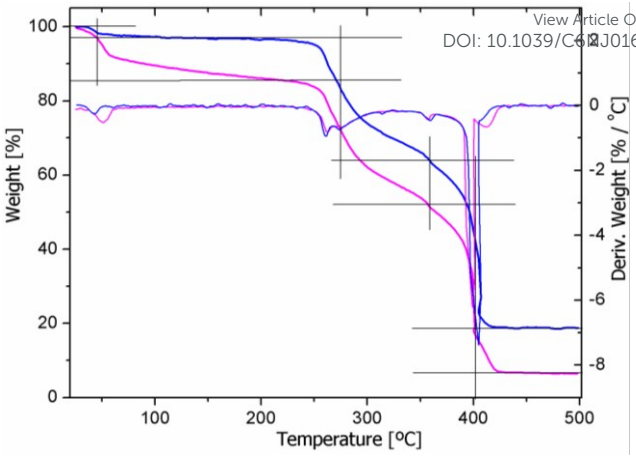

Fig. 12: Comparison between thermogravimetric and differential thermogravimetric curves for compounds **1** (blue line) and **2** (violet line). Measurements run under N_2 at 5 °C/min.

The second transition corresponds to the loss of 36.46% (215-350 °C) is assigned to nitrates, lithium entities and lattice water (calc. 34.38 %). Finally, the last transition of 44.13 % (350-440 °C) is assigned to the loss of *tpmc* ligand (calc. 47 %) and the residue of 6.5 % corresponds to NiO (calc. 6.3 %). These assignments are in agreement with those reported for the analogous copper-*tpmc* compound, [36] and nickel nitrate. [37]

Thermogram of **1** exhibits a very little loss of 2.35 % (≈50 °C), corresponding to 1.6 water molecules (-2.5 %). This little amount of water, is due to the high affinity of **1** towards water (during its manipulation, even though is made under nitrogen). The comparison between TGA and DGA curves for **1** and **2** is shown in figure 12.

TGA curves for compounds **1** and **2** are the same from 200 °C to the end; this being consistent with previous findings, giving an extra evidence that after heating compound 2, this becomes compound 1.

Additionally, the thermograms for **1** and **2** were carried out under air, as well as under nitrogen. The observed transitions were the same in both cases.

N_2 adsorption-desorption isotherm for **1** was acquired to determine its microstructural features. Figure S7 (ESI†) shows the resulting curve. According to the IUPAC classification, [21] it corresponds to a type IIb isotherm with a very narrow hysteresis loop, feature that is typical for a macroporous adsorbent, which allows unrestricted multimolecular adsorption, favoured at high relative pressures. The observed hysteresis is also characteristic of a chemisorption process where a slight change in the active surface takes place.

The resulting isotherms were analysed by using the BET and BJH models. [21] According to BET the surface area of **1** was found 4.24 m^2/g, the total pore volume 0.015 cm^3/g and the average pore diameter 14.48 nm. However, according to BJH analysis, the average pore diameter was aleatory distributed. Therefore, the value found by BET studies, corresponds to the size among particles of the bulk solid. In order to understand this behaviour, adsorption-desorption measurements at high pressure (until 4.5 MPa), by using CO_2 flow, were performed.

View Article Online
DOI: 10.1039/C6NJ01621A

The resulting isotherm is shown in figure S8 (ESI†). A continuous adsorption increment was observed, indicating the presence of big size porous, most probably, located in the outer layer of the compound. [38]

To get a deeper insight into the adsorption process, water vapour isotherms of complex **1** were obtained as a function of the humidity percentage at 303, 313 and 333 K, using nitrogen as carrier gas (figure 13). The adsorption process began at the same relative humidity percentage (RH %) and the saturation was reached almost at the same weight percentage, independently of applied the temperature. The differences between curves were the total weight gain favoured at lower temperature. At 303 K, the maximum adsorbed water was 5 % wt, while at 313 K it was only of 3 % wt. The gained weight and the fact that the curve did not end at the starting point, is attributed to a chemisorption process.[21, 39] In contrast, at 333 K, the curve returned to the starting point, indicating that all the adsorbed water was completely desorbed, which is characteristic of a physisorption process. [21, 39] Therefore, at 333 K the energy of the chemisorption was overcome.

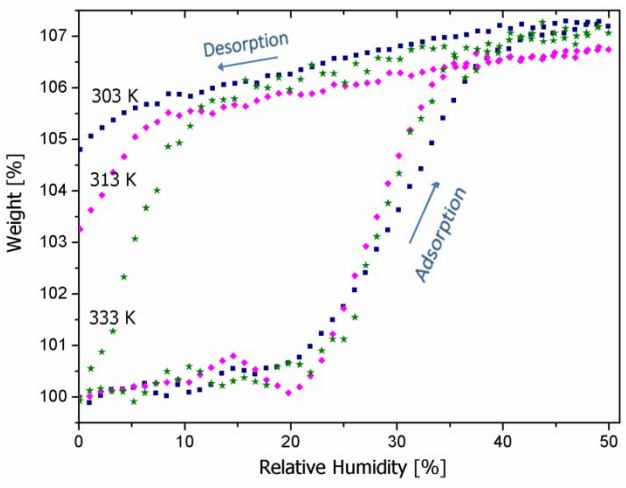

Fig. 13: Water adsorption – desorption isotherms of complex **1** measured at 30, 40 and 60 °C, using N_2 as carrier gas.

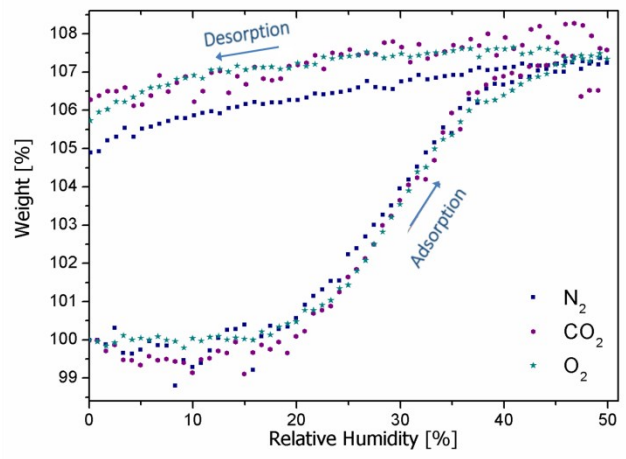

Fig. 14: Water adsorption – desorption isotherms of complex **1**, using carrier gases: N_2, CO_2 and O_2, measured at 303 K.

A second kind of water vapour isotherms was performed for **1** at 303 K using different carrier gases, such as O_2 and CO_2. The corresponding curves are shown in figure 14. A slight increase in the maximum water adsorbed was observed when CO_2-H_2O or O_2-H_2O flows were used in comparison to the N_2-H_2O flow. This is indicative that either O_2 or CO_2 can also be adsorbed by **1**. Then, the binuclear nickel (II) compound **1**, is able to adsorb carbon dioxide, dioxygen, nitrogen and water vapour, however, only the adsorption of water changes the original blue colour of **1** into the violet colour of **2**.

Interestingly, analogous compounds based on cobalt and copper, published elsewhere, [7-10, 13] did not present adsorption properties, leading us to conclude this phenomenom is inherent of nickel. [1, 35]

The morphological characteristics of the binuclear nickel (II) compound, after the adsorption process, were studied by scanning electron microscopy coupled to Energy-dispersive X-ray spectroscopy (SEM-EDS). Figure 15 shows corresponding micrographs and figure S9 (ESI†) show the EDS analysis results.

Two different phases were identified. The irregular polyhedron-shaped particles were assigned to compound **1**, according to the X-ray identification and composition determined by EDS. These dense particles, of about 10 μm, present a corrugated surface which could be associated with a large surface area and therefore with the capacity of adsorption. [40, 41] The second phase is a set of small particles of about 0.1 μm corresponding to a phase rich in oxygen, which was assigned to compound **2**. The observed agglomeration is related to a small surface area, which is expected after the adsorption process took place. [40, 41] Elemental percentages found by EDS agree with those found by elemental analysis (see experimental section).

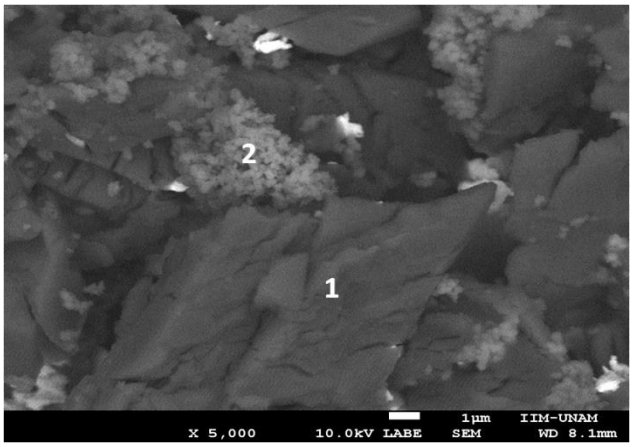

Fig. 15: Backscattered electron image for the complex **2**. The different phases observed correspond to compounds **1** and **2**.

Conclusion

Two novel flexible supramolecular solids based on binuclear nickel(II) complexes with *tpmc* and nitrate were obtained. The blue compound **1**, $[Ni_2(tpmc)(\mu\text{-}NO_3)](NO_3)_3(H_2O)_2[LiNO_3{\cdot}3H_2O]$, adsorbs water leading to the violet

compound **2**, $[Ni_2(tpmc)(\mu\text{-}NO_3)]_2[Ni_2(tpmc)(\mu\text{-}NO_3)Li(NO_3)_2OH]_2(LiOH(H_2O)_3)_2(NO_3)_8(H_2O)_{13}\bullet 32H_2O$.

Nickel (II) ions in both compounds are in an octahedral environment, due to a non-common coordination mode for nitrate, acting as a tetradente ligand in **1**, described as μ^2-nitrate-1κ^1O,2κ^1O,3κ^2O; while as a pentadente ligand in **2**, described as μ^3-nitrate-1κ^1O,2κ^2O,3κ^2O. These are the first crystal structures of six-coordinated nickel (II) complexes with *tpmc* ligand. It is also the first report where *tpmc* compounds are involved in a reversible gas-adsorption phenomenon. The adsorption of water by **1** changes its crystal network, leading to a reversible structural phase transition, accompanied by a colour change, from the monoclinic structure of **1**, to the triclinic of **2**, characterizing them as flexible supramolecular networks. This structural phase transition was also confirmed by XRPD.

Crystalline packings of **1** and **2**, contain lithium entities, which play a critical role in the stabilization of the supramolecular networks. The incorporation of water induces a reaction of ligand exchange consisting of a coordination of a lithium entity towards the bridging nitrate, process that is completely reversible when water is removed. Also the incorporation of the lithium entity into the coordination sphere of nickel in complex **2** changes its electronic environment, resulting in the observed colour change.

Two phases were identified by SEM-EDS analysis, that according to their morphology and composition were assigned to **1** and **2**.

Adsorption-desorption isotherms at low and high pressure indicated **1** has capacity of gases adsorption. Dynamic water vapour isotherms confirms the binuclear nickel (II) complexes adsorbs water through a chemisorption process. At 333 K the chemisorption energy is overcome and a physisorption takes over. Therefore, at high temperature all adsorbed water is completely desorbed, confirming the reversibility of the adsorption phenomenon.

The binuclear nickel (II) compound **1**, has also the ability to adsorb carbon dioxide, dioxygen and nitrogen, according with the isothermal measurements; nevertheless, only the adsorption of water changes the original blue colour of **1** into the violet colour of **2**, property which might be useful for the development of molecular sensors.

Acknowledgements

We gratefully acknowledge the financial support of by CONACyT, Projects 128921 and 129293, DGAPA-UNAM, Projects IN231111 and IN106014, and finally to BISNANO Project 2011. B.L.R.H thanks to CONACyT for the Ph.D. scholarship 240230. We thank to V.H. Lemus Neri, N. López Balbiaux and M. Gutiérrez Franco from USAI-UNAM (*Unidad de Servicios de Apoyo a la Investigación*, Facultad de Química, UNAM) for their analytical services and technical assistance; to S. Barragán Rosendo from Departamento de Diseño y Medios Audiovisuales FQ-UNAM; to A. Morales Espino for his technical support from *Laboratorio de Refinamiento de Estructuras Cristalinas* (LAREC) of Instituto de Física, UNAM, and to Dr. Heriberto Pfeiffer and his work group for their help with the adsorption measurements.

View Article Online
DOI: 10.1039/C6NJ01621A

References

1 (a) R. Miyake, C. Kuwata, Y. Masumoto, *Dalton Trans.*, 2015, **44**, 2993; (b) M. Almasi, V. Zelenak, M. Opanasenko, J. Cejka, *Dalton Trans.*, 2014, **43**, 3730.
2 a) J. Cejka, A. Corma, S. Zones, *Zeolites and Catalysis, Synthesis, Reactions and Applications*; Wiley-VCH, Weinheim, Germany, 2010. b) P. Wright, M. Maple, A. Slawin, V. Patinec, A. Aitken, S. Welsh, P. Cox, *J. Chem. Soc*., *Dalton Trans*., 2000, 1243.
3 a) Steed J. W., Atwood J. L., *Supramolecular Chemistry*, Second Edition, John Wiley and Sons, UK 2009. b) Seiffert S. (Editor), *Supramolecular polymer networks and gels*, Advances in polymer science 268, Springer, Switzerland 2015. c) Steed J. W., Turner D. R., Wallace K. J., *Core concepts in supramolecular chemistry and nanochemistry*, John Wiley and Sons, UK 2007.
4 J. Boonmak, M. Nakano, N. Chaichit, C. Pakawatchai, S. Youngme, *Dalton Trans.*, 2010, **39**, 8161.
5 H. Furukawa, F. Gándara, Y. Zhang, J. Jiang, W. Queen, M. Hudson, O. Yaghi, *J. Am. Chem. Soc.*, 2014, **136**, 4369.
6 J. Narayanan, M. Sosa-Torres, R. Toscano, *J. Chem. Crystall*., 2001, **31**, 129.
7 J. Narayanan, A. Solano-Peralta, V. Ugalde-Saldivar, R. Escudero, H. Hopfl, M. Sosa-Torres, *Inorg. Chim. Acta,* 2008, **361**, 2747.
8 G. Vuckovic, M. Antonijevic-Nikolic, T. Lis, J. Mrozinski, M. Korabik, D. Radanovic, *J. of Molecular Structure*, 2008, **872**, 135.
9 G. Vuckovic, E. Asato, N. Matsumoto, *Inorganica Chimica Acta*, 1990, **171**, 45.
10 N. Alcock, P. Karapulli, P. Balakrishnan, P. Moore, *J. Chem. Soc. Dalton Trans*., 1986, 1743.
11 M. Mikuriya, I. Murase, E. Asato, S. Kida, *Chem. Lett.*, 1989, **18**, 497.
12 H. Harada, M. Kodera, G. Vuckovic, N. Matsumoto, S. Kida, *Inorg. Chem.,* 1991, **30**, 1190.
13 B. Petkovic, M. Milcic, D. Stankovic, I. Stambolic, D. Manojlovic, V. Jovanovic, S. Sovilj, *Electrochimica Acta,* 2013, **89**, 680.
14 A. Vogel, *A text-book of quantitative Inorganic Analysis*, Longmans Green and Co., London, 2nd edition, 1951.
15 a) Oxford Diffraction *CrysAlis CCD* and *CrysAlis RED*, Oxford Diffraction Ltd, Abingdon, England, 2010. b) C. Clark, J. Ried, *Acta Cryst. Sect. A*, 1995, **51**, 887.
16 a) Bruker AXS Inc., *SAINT Version 8.27A*, Madison Wisconsin, USA; 2013. b) Bruker AXS Inc., *SADABS*, Madison Wisconsin, USA, 2012.
17 G. M. Sheldrick, *Acta Cryst. Sect. C.,* 2015, **71**, 3.
18 a) L. J. Farrugia, *J. Appl. Crystallogr.*, 1997, **30**, 565.; b) L. J. Farrugia, *J. Appl. Crystallogr.*, 1999, **32**, 837;
19 a) C. Macrae, I. Bruno, J. Chisholm, P. Edgington, P. McCabe, E. Pidcock, L. Rodriguez-Monge, R. Taylor, J. Van de Streek, P. A. Wood, *J. Appl. Cryst.* 2008, **41**, 466; b) Crystal Impact Gbr, *Diamond* Version 4.0.4, Bonn Germany, 2015.
20 A. Altomare, C. Cuocci, C. Giacovazzo, A. Moliterni, R. Rizzi, N. Corriero, A. Falcicchio, *J. Appl. Cryst.*, 2013, **46**, 1231.
21 F. Rouquerol, J. Rouquerol, K. Sing, P. Lewellyn, G. Maurin, *Adsorption by Powders and Porous Solids, Principles, Methodology and Applications*, Second edition, Academic Press, UK 2014.
22 A. P. Lever, *Inorganic Electronic Spectroscopy,* Second Edition, Elsevier, Netherlands 1984.

View Article Online
DOI: 10.1039/C6NJ01621A

23 G. Socrates, *Infrared Characteristic Group Frequencies, Tablas and Charts*, John Wiley and Sons, Second Edition, UK 1994.
24 K. Nakamoto, *Infrared and Raman Spectra of Inorganic and Coordination Compounds*, John Wiley and Sons, UK 1986
25 A. M. Appel, R. Newell, D. L. DuBois, R. DuBois, *Inorg. Chem.*, 2005, **44**, 9, 3046.
26 M. Albrecht, O. Osetska, R. Frohlich, *Dalton Trans.*, 2005, 3757.
27 N. G. Connelly, T. Damhus, R. M. Hartshorn, A. T. Hutton, Nomenclature of Inorganic Chemistry IUPAC Recommendations 2005, *International Union of Pure and Applied Chemistry RSC Publishing*, UK 2005.
28 K. Tugashov, D. Gribanyov, F. Dolgushin, A. Smolyakov, A. Peregudov, M. Minacheva, B. Strunin, I. Tikhonova, V. Shur, *J. Organometallic Chem.*, 2013, **747**, 167.
29 S. She, Y. Chen, M. Zaworotko, W. Liu, Y. Cao, J. Wua, Y. Li, *Dalton Trans*., 2013, **42**, 10433.
30 B. Day, J. Clayden, R. Layfield, *Organometallics*, 2013, **32**, 4448.
31 L. Pratt, A. Streitwieser, *J. Org. Chem.,* 2000, **65***,* 290.
32 T. Kremer, F. Hampel, F. Knoch, W. Bauer, A. Schmidt, P. Gabold, M. Schütz, J. Ellermann, P. Schleyer, *Organometallics,* 1996, **15**, 4776.
33 G. Cakmak, J. Nuss, M. Jansen M., *Z. Anorg. Allg. Chem*., 2009, **635**, 631.
34 M. C. Etter, *Acc. Chem. Res*., 1990, **23**, 120.
35 a) R. Miyake, M. Shionoya, *Chem. Commun*., 2012, **48**, 7553. b) R. Miyake, M. Shionoya, *Inorg. Chem.*, 2014, **53**, 5717.
36 S. Sovilj, K. Babic-Samardzija, D. Minic, *Thermochimica Acta*, 2001, **370**, 29.
37 W. Brockner, C. Ehrhardt, M. Gjikaj, *Thermochimica Acta*, 2007, **456**, 64.
38 P. R. Díaz-Herrera, M. J. Ramírez-Moreno, H.Pfeiffer, Chemical Engineering Journal, 2015, **264**, 10.
39 a) H. Pfeiffer, P. Bosh, *Chem. Mater.*, 2005, **17**, 1704; b) H. Mosqueda, C. Vazquez, P. Bosh, H. Pfeiffer, *Chem. Mater.*, 2006, **18**, 2307.
40 Y. Xian-Sheng, S. Miao, Z. Qin-Hui, Y. Jian-Guo, *Ind. Eng. Chem. Res.*, 2010, **49**, 6593.
41 R. Rodríguez-Mosqueda, H. Pfeiffer, *J. Phys. Chem. C*, 2013, **117**, 13452.

View Article Online
DOI: 10.1039/C6NJ01621A

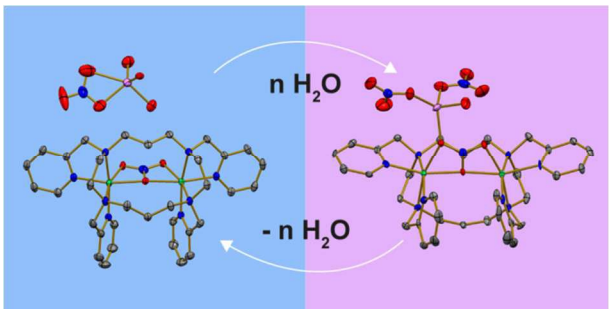

A reversible reaction of ligand-exchange in a nickel(II)-*tpmc* complex, promoted by water adsorption, results in a structural phase transition accompanied by colour change.